Design of Spatial Disposition of Anionic Porphyrins in Matrices of Ammonium Bilayer Membranes

Yuichi Ishikawa and Toyoki Kunitake*

Contribution No. 923 from the Department of Organic Synthesis, Faculty of Engineering, Kyushu University, Fukuoka 812, Japan. Received May 2, 1990

Abstract: A methodology to place charged porphyrin derivatives in specific spatial arrangements in matrices of ammonium bilayer membranes was explored. Aqueous mixtures of anionic copper(II) porphyrins and bilayer dispersions of single-chain and double-chain ammonium amphiphiles were cast on Teflon sheets to produce regular multilayer films. The orientation of doped copper(II) porphyrins was determined by anisotropies of ESR spectral patterns that were dependent on the disposition of the cast film in the magnetic field. Quantitative estimates of the porphyrin orientation were made possible by elaborate computer simulation of the observed spectra. The mode of porphyrin orientation is determined by the distribution of anionic substituents on guest porphyrins and the supramolecular structure of host bilayers. Type III porphyrins, which possess evenly distributed anionic substituents, are incorporated horizontally on the ammonium bilayer surface. Type I porphyrins, in which anionic substituents are localized on one side of the porphyrin ring, are incorporated into the spacer portion of the bilayer parallel to the molecular axis in the case of the double-chain ammonium amphiphile. In contrast, these porphyrins cannot penetrate into the bilayer interior of the single-chain amphiphile and show random incorporation. A type II porphyrin with three sulfonate substituents gives a horizontal orientation on the nonpenetrable bilayer of the single-chain amphiphile and a random orientation in the bilayer of the double-chain amphiphile. The standard deviation of the porphyrin orientation was always 15°, implying that the orientational fluctuation is derived from undulation of the cast film. The microscopic orientation is thus highly specific. The present findings should be instrumental in designing biomimetic functional systems.

Introduction

Biochemical processes occurring in the biomembrane are in many cases conducted by cooperative action of functional molecules (or parts of molecules) that are precisely disposed in the matrix membrane. One outstanding example is given by porphyrin functional units that are placed in the photosynthetic reaction center.[1] Therefore, specific incorporation of metalloporphyrins in biomimetic membranes and their functions have been of great interest. van Esch Roks and Nolte[2] incorporated a synthetic model system of cytochrome P-450 that includes a manganese(II) porphyrin in polymerized vesicles of a double-chain ammonium amphiphile and studied its monooxygenase activity. Groves and Neumann used a steroidal porphyrin to conduct regioselective epoxidation in phospholipid vesicles.[3] Tsuchida and co-workers[4] introduced polymerizable porphyrins and phosphocholine porphyrins into polymerizable phospholipid vesicles and examined the oxygen-carrier property. The spatially defined disposition of multiple porphyrins is essential in dealing with transmembrane electron transport. Dannhauser et al.[5] studied this process by using manganese(II) tetraphenylporphyrins whose distances from the phospholipid bilayer surface are determined by the poly(ethylenimine) ligand. Nango et al.[6] used phospholipid-linked manganese porphyrins for this purpose. Stacked zinc triporphyrin was inserted into planar lipid bilayers (BLM) as molecular wire to induce electron flux across the membrane.[7] Murakami et al. studied catalysis by a hydrophobic vitamin B_{12} in synthetic bilayer matrices.[8]

Direct determination of the spatial disposition of porphyrins has been conducted by using the macroscopic anisotropy of the matrix bilayer such as multibilayered cast films or BLM's of phospholipids. For instance, the macroscopic orientation of diamagnetic porphyrins like chlorophyll *a* was examined by polarized absorption spectroscopy[9-13] and that of paramagnetic porphyrins such as heme in cytochromes or synthetic metalloporphyrin was elucidated by the magnetic anisotropy of ESR spectra.[3,14-19]

Most of these spectroscopic attempts are qualitative at best. Like the inference of Fuhrhop and Mathieu,[20] they could only deal with crude orientations such as whether the porphyrin ring is parallel or normal to the membrane surface. Exceptional examples of the quantitative estimate were provided by Poole et al.[14] and Blum et al.[15] They determined the tilt angle of the metalloporphyrin ring in lipid bilayers from comparisons of anisotropic ESR spectra and their computer simulations.

We have been interested in construction of organized functional systems in synthetic bilayer membranes. Porphyrins are particularly attractive functional units if one considers their versatile roles in the biochemical system. The past methodology of porphyrin orientation has serious disadvantages. One is limited preciseness of orientation. The observed orientations are only approximate. It would be difficult to construct a multiple porphyrin system of fixed spatial disposition on the basis of ap-

(1) Deisenhofer, J.; Epp, O.; Miki, K.; Huber, R.; Michel, H. *Nature* **1985**, *318*, 618.
(2) van Esch, J.; Roks, M. F. M.; Nolte, R. J. M. *J. Am. Chem. Soc.* **1986**, *108*, 6093.
(3) Groves, J. T.; Neumann, R. *J. Am. Chem. Soc.* **1989**, *111*, 2900.
(4) Tsuchida, E.; Nishide, H.; Yuasa, M.; Hasegawa, E.; Eshima, K.; Matsushita, Y. *Macromolecules* **1989**, *22*, 2103. Tsuchida, E.; Nishide, H.; Yuasa, M.; Babe, T.; Fukuzumi, M. *Macromolecules* **1989**, *22*, 66.
(5) Dannhauser, T. J.; Nango, M.; Oku, N.; Anzai, K.; Loach, P. A. *J. Am. Chem. Soc.* **1986**, *108*, 5865.
(6) Nango, M.; Mizuwawa, A.; Miyake, T.; Yoshinaga, J. *J. Am. Chem. Soc.* **1990**, *112*, 1640.
(7) Seta, P.; Bienvenue, E.; Maillard, P.; Momenteau, M. *Photochem. Photobiol.* **1989**, *49*, 537.
(8) Murakami, Y.; Hisaeda, Y.; Ohno, T. *Bull. Chem. Soc. Jpn.* **1984**, *57*, 2091.
(9) van Gurp, M.; van der Heide,; Verhagen, J.; Pitters, T.; van Ginkel, G.; Levine, Y. K. *Photochem. Photobiol.* **1989**, *49*, 663.
(10) Fragata, M.; Norden, B.; Kurucsev, T. *Photochem. Photobiol.* **1988**, *47*, 133.
(11) Hoff, A. J. *Photochem. Photobiol.* **1974**, *19*, 51.
(12) Steinemann, A.; Stark, G.; Lauger, P. *J. Membr. Biol.* **1972**, *9*, 177.
(13) Cherry, R. J.; Hsu, K.; Chapman, D. *Biochim. Biophys. Acta* **1972**, *267*, 512.
(14) Poole, R. K.; Blum, H.; Scott, R. I.; Collinge, A.; Ohnishi, T. *J. Gen. Microbiol.* **1980**, *119*, 145.
(15) Blum, H.; Harmon, H. J.; Leight, J. S., Jr.; Salerno, J. C.; Chance, B. *Biochim. Biophys. Acta* **1978**, *502*, 1.
(16) Erecinska, M.; Wilson, D. F.; Blasie, J. K. *Biochim. Biophys. Acta* **1978**, *501*, 63.
(17) Blasie, J. K.; Erecinska, M.; Samuels, S.; Leigh, J. S. *Biochim. Biophys. Acta* **1978**, *501*, 33.
(18) Erecinska, M.; Wilson, D. F.; Blasie, J. K. *Biochim. Biophys. Acta* **1978**, *501*, 53.
(19) Blum, H.; Salerno, J. C.; Leigh, J. S., Jr. *J. Magn. Reson.* **1978**, *30*, 385.
(20) Fuhrhop, J.-H.; Mathieu, J. *Angew. Chem., Int. Ed. Engl.* **1984**, *23*, 100.

0002-7863/91/1513-621$02.50/0

Chart I

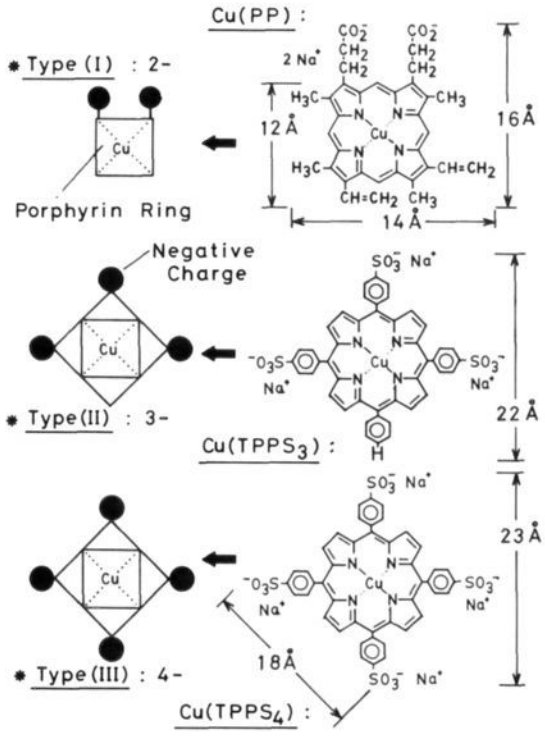

proximate orientations of individual porphyrins. The unsatisfactory orientation is apparently derived from the insufficient ordering of matrix bilayers. Phospholipids of the biological origin would not produce highly regular multibilayers.

The second disadvantage is the lack of molecular design. Porphyrin derivatives used in the previous examples either are of the biological origin or are modified only to ensure efficient incorporation into lipid bilayers. The molecular design intended for precise orientation was lacking or insufficient. Since the mode of porphyrin incorporation should be affected by molecular and supramolecular structures of host bilayer and guest porphyrin, it is desirable to study the structure–orientation relationship for systematically varied combinations of bilayer and porphyrin.

We reported previously that negatively charged, planar Cu(II) complexes are incorporated into cast multibilayer films of ammonium amphiphiles in specific manners.[21] According to ESR spectral anisotropies, hexaanionic $Cu(Tiron)_2$ was placed horizontally on the bilayer surface and monoanionic Cu(Zincon) was inserted on the bilayer along the molecular axis (Chart III). These anisotropic orientations can be interpreted quite simply in terms of electrostatic and hydrophobic stabilizations. The porphyrin orientation in bilayers would be similarly manipulated, because this new concept should be applicable to any planar molecules. Many of the synthetic bilayer membranes give cast multibilayer films with structural regularity superior to that of biolipid molecules. Their versatile molecular structures provide additional advantages for proper molecular design of host membranes.

We describe in this paper how the orientation of anionic copper(II) porphyrins in ammonium bilayers can be controlled in straightforward manners. Improved computer simulation of ESR spectra and the enhanced regularity of multibilayer films give rise to precise determination of the porphyrin orientation.

Results and Discussion

Molecular Design of Guest Porphyrins and Host Bilayers. The porphyrin derivatives employed in this study are classified into type I, type II, and type III, as shown in Chart I. The relationship between the molecular structure of guest porphyrins and their orientation in host bilayer membranes can be established in terms

(21) Ishikawa, Y.; Kunitake, T. *J. Am. Chem. Soc.* **1986**, *108*, 8300.

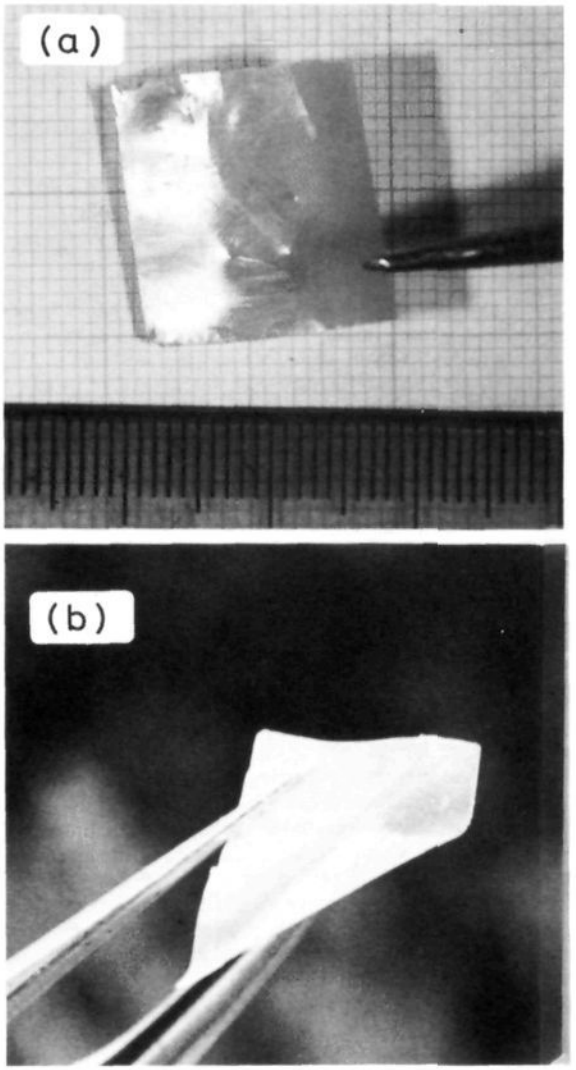

Figure 1. Photographs of cast multibilayer films: (a) stiff C_8-Azo-C_{10}-N^+ film; (b) flexible $2C_{14}$-Glu-ph-C_6-N^+ film.

of this classification. It should be applicable to other planar guest molecules with charged substituents.

In type I structures, negatively charged groups are localized only in one side of the planar hydrophobic core and the hydrophobic area and the hydrophilic area are closely separated. Protoporphyrin (PP) is a representative case. The type II structure is represented by $TPPS_3$, and the charged substituents are unsymmetrically located in three sides of the porphyrin ring. $TPPS_4$ is one of the type III compounds that possess symmetrically distributed charged groups.

These porphyrins were converted to the corresponding Cu(II) complexes in order to determine their orientations by the angular dependence of ESR spectra relative to the direction of the magnetic field. The copper(II) porphyrins are ideal as paramagnetic probes for the following reasons: (1) The structure of the ligand moiety remains unaltered upon metal complexation. (2) The magnetic anisotropy is expressed unmistakably in ESR spectra, unlike nitroxide probes and high-spin Fe(III) complexes. (3) The choice of the experimental conditions is flexible, since the spectral observation can be made at room temperature and under the aerobic conditions.

The host bilayer membranes used in this study are C_8-Azo-C_{10}-N^+ and $2C_{14}$-Glu-ph-C_6-N^+ (Chart II). The most important factor for their use is that they form cast films that display high regularities of the multilayer structure together with self-supporting strengths sufficient for ESR experiments. The second reason is that the mode of molecular organization in the two cast films is

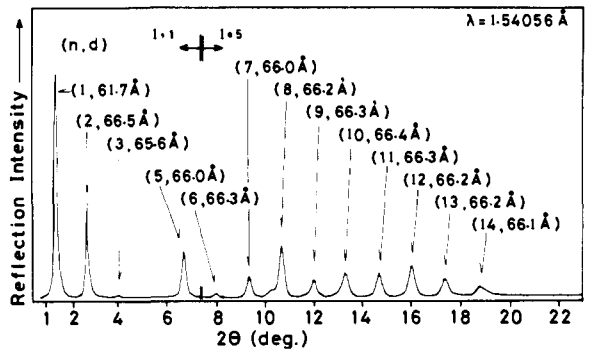

Figure 2. X-ray diffraction pattern (reflection mode) of cast multibilayer film of $2C_{14}$-Glu-ph-C_6-N^+: *n*, the order of diffraction; *d*, bilayer thickness; θ, angle between incident beam and the film surface; λ, X-ray wavelength. The *n* and *d* values are given in parentheses. The data satisfy the Bragg equation.

Chart II

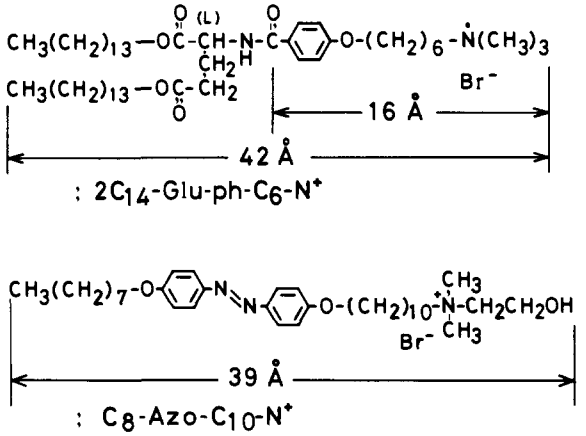

very different, as mentioned in the following text. As a result, the effect of the host bilayer structure on the guest orientation is clearly seen.

Structure of Cast Film. A photograph of a cast film of single-chain amphiphile C_8-Azo-C_{10}-N^+ is shown in Figure 1a. This yellow film is rather stiff and brittle, though self-supporting. Good care was required for its handling. The cast film is made of a regular multibilayer structure.[22] The exact molecular arrangement of the unit bilayer has been determined by Okuyama et al.[23] by single-crystal X-ray diffraction. The amphiphile assumes an interdigitated bilayer structure with component molecules aligned perpendicular to the membrane surface. A stable cast film was also obtained from $2C_{14}$-Glu-ph-C_6-N^+,[24] as shown in Figure 1b. This is a slightly turbid, highly flexible film. It does not break when bent gently. An X-ray diffraction pattern (reflection mode) of this film is shown in Figure 2. A series of sharp peaks up to the 14th order of diffraction were obtained with a spacing of 66.2 Å. It is obvious, as also noted before for a related amphiphile of $2C_{14}$-Glu-C_{11}-N^+,[25] that a highly regular multibilayer film is formed. The extended molecular length of this amphiphile that is estimated from its CPK model is 42–43 Å. The observed bilayer thickness is much smaller than 2 times the CPK molecular length (85 Å); therefore, the amphiphile molecule must be arranged in a tilted manner in the bilayer.

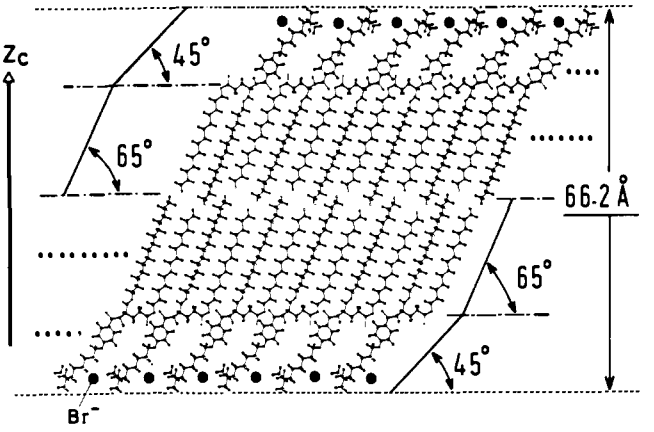

Figure 3. Plausible model of the molecular packing of the bilayer of $2C_{14}$-Glu-ph-C_6-N^+, as produced by electron-density matching of the X-ray diffraction data of Figure 2. The plane of the benzene ring is arbitrarily set in the plane of the two alkyl chains. When the benzene plane is assumed to be in the perpendicular disposition, the tilt angles for the spacer and tail chains become slightly greater: 50° for the spacer and 75° for the tail.

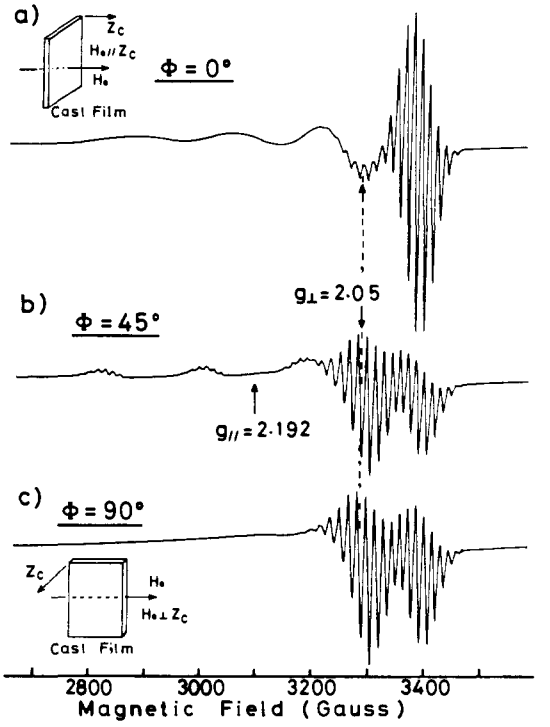

Figure 4. Observed ESR spectra of Cu(PP) embedded in a cast film of $2C_{14}$-Glu-ph-C_6-N^+: room temperature; ν = 9.455 GHz; [Cu(PP)]:[$2C_{14}$-Glu-ph-C_6-N^+] = 1:58. Key: (a) $\Phi = 0°$, (b) $\Phi = 45°$, (c) $\Phi = 90°$.

Okada[26] conducted a simulation of the regular molecular layer according to the procedure of Harada et al.[27] The relative structure amplitudes were estimated from the diffraction intensities, and the corresponding structure amplitudes were compared with the observed amplitudes of the diffraction. A plausible model thus obtained (see Figure 3) has the spacer and tail chains tilted against the bilayer surface by 45° and 65°, respectively. These different extents of tilting arise in order to attain close packing at both the spacer and tail portions. The spacer portion can accommodate various guest molecules through small conformational changes. The C_6 spacer was selected, as the distance of ~16 Å from the connector (glutamate residue) to the ammonium

(22) Kunitake, T.; Shimomura, M.; Kajiyama, T.; Harada, A.; Okuyama, K.; Takayanagi, M. *Thin Solid Films* **1984**, *121*, L89.
(23) Xu, G.; Okuyama, K.; Shimomura, M. *Polym. Prepr. Jpn.* **1989**, *38*, 2407.
(24) An aqueous bilayer dispersion pf $2C_{14}$-Glu-ph-C_6-N^+ (1 mM, sonicated) gives vesicular (diameter ca. 1000–3000 Å) and helical (pitch 1000–1500 Å; width ca. 500 Å) morphologies. The regular molecular assemblage in bilayer gives rise to enhanced circular dichroism ($[\theta]_{262nm} = -4 \times 10^5$ deg·cm^{-2}/dmol, 25 °C).
(25) For a cast film of $2C_{14}$-Glu-ph-C_6-N^+ that possesses a shorter spacer methylene, see: Asakuma, S.; Kunitake, T. *Chem. Lett.* **1989**, 2059.
(26) Okada, H., Molecular Architecture Project, Japan. Unpublished results.
(27) Harada, A.; Okuyama, K.; Kumano, A.; Kajiyama, T.; Takayanagi, M.; Kunitake, T. *Polymn. J.* **1986**, *18*, 281.

Table I. Experimental ESR Parameters for Copper Porphyrins

matrix	complex	$g_{\parallel}$	$g_{\perp}$	$A_{\parallel} \times 10^4$ (cm^{-1})
$2C_{14}$-Glu-ph-C_6-N^+ [a]	Cu(TPPS$_4$)	2.193	2.06	201
	Cu(TPPS$_3$)	2.201	2.06	201
	Cu(PP)	2.192	2.05	205
	Cu(ChP)	2.188	2.05	200
	Cu(PhCS$_4$)	2.151	*b*	212
	Cu(T(5-ST)P)	2.200	2.06	201
H_2TPP	Cu(TPP)[c]	2.187	2.045	202
H_2PP	Cu(PP)[d]	2.192	2.054	203
H_2PhC	Cu(PhC)[e]	2.160	2.045	218

[a] Room temperature. Values of $A_{\perp}$, $A^N_{\parallel}$, and $A^N_{\perp}$ were not directly measurable from the spectra due to overlapping signals. [b] Unmeasurable due to the broadening signal of stacked species. [c] 77 K.[40] [d] 131 K.[40] [e] Room temperature.[40]

head is close to that between the hydrophilic substituent and the farthest rim of the porphyrin ring.

Experimental ESR Spectra of Cu(PP) Embedded in a Cast Film of $2C_{14}$-Glu-ph-C_6-N^+. Figure 4 demonstrates ESR spectra of Cu(PP) embedded in a highly regular cast film of $2C_{14}$-Glu-ph-C_6-N^+. The spectral shapes are strongly affected by the angle between the magnetic field (H_0) and the film plane (Zc axis). When the angle (Φ) between H_0 and the film Z_C axis is 45°, the hyperfine structure (hfs) due to Cu(II) ($S = {}^1/_2$, $I_{Cu} = {}^3/_2$) and the superhyperfine structure (shfs) due to the four equivalent coordinating nitrogens ($I_N = 1 \times 4 = 4$) are clearly seen (Figure 4b). As given in Table I, ESR parameters (g and A values) estimated from this spectrum agree with those of Cu(PP) in a matrix of the PP ligand within the experimental error. When the film plane is placed normal to the magnetic field (i.e., $H_0 \parallel Z_C$), the $g_{\parallel}$ components give a broad, undulating spectrum at 2800–3300 G without shfs. Weak signals due to the $g_{\perp}$ components and remarkably strong extra peaks are also present at 3200–3300 and at 3330–3470 G, respectively.

On the other hand, when the film plane is parallel to the magnetic field ($H_0 \perp Z_C$, Figure 4c), the $g_{\parallel}$ signals become even broader and the intensities of the $g_{\perp}$ components and the extra peaks are slightly enhanced over those of Figure 4b.

These anisotropic ESR spectra did not change at all by in-plane rotation or out-of-plane (by 180°) rotation of the film in the ESR cavity. Therefore, the magnetic anisotropy depends solely on the angle Φ between H_0 and Z_C, and there is no anisotropy within the X_C–Y_C plane. This ESR anisotropy should be in principle the same as that we observed for Cu(Zincon), which showed shfs of the two coordinating nitrogens.[21] However, the precise molecular orientation of Cu(PP) can be inferred in satisfactory reliability only upon spectral simulation.

Simulation Procedure of ESR Spectra of Copper(II) Porphyrins. The following assumptions, which we believe to be reasonable, were made in conducting the spectral simulation:

(1) The proper axis of rotation is coincident with the $g_{\parallel}$ axis of the Cu(II) complex.

(2) The $\bar{g}_{\parallel}$ axes (averaged $g_{\parallel}$ axis) are oriented in a regular manner with respect to the film Z_C axis, but it is randomly oriented within the X_C–Y_C plane.

(3) The orientation of the $g_{\parallel}$ axis of individual Cu(II)–porphyrin molecules obeys the normal (Gaussian) distribution function with a standard deviation σ.

Our simulation program, which is based on these assumptions, is a modified and upgraded version of programs independently developed by Matsuda[28] and Chikira.[29] Our program adopts for a magnetically diluted Cu(II)–porphyrin complex the first and second terms of perturbation theory for hyperfine interactions and the first term for superhyperfine interactions. The presence of

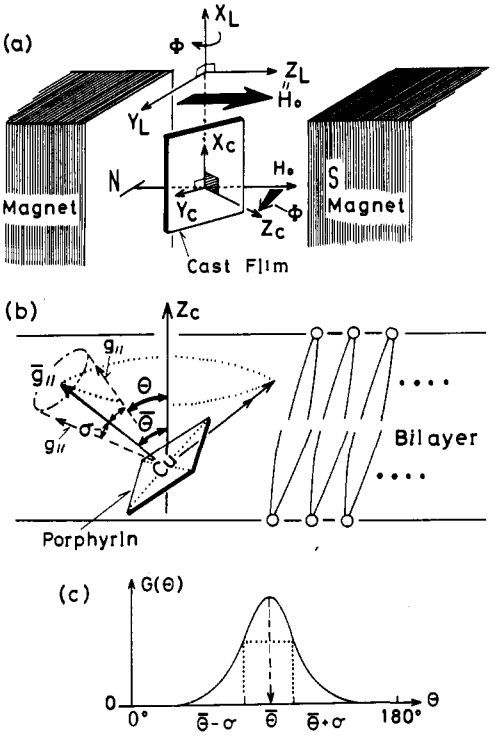

Figure 5. Relationship among the laboratory coordinate system (X_L, Y_L, Z_L), cast-film coordinate system (X_C, Y_C, Z_C), and $\bar{g}_{\parallel}$ axis. The spatial disposition of $\bar{g}_{\parallel}$ (mean $g_{\parallel}$) axis in a cast film was characterized by Φ (angle for Z_C and H_0), $\bar{\theta}$ (angle for $\bar{g}_{\parallel}$ and Z_C), and σ (standard deviation of $\bar{g}_{\parallel}$). See Experimental Section for the details. Key: (a) Sketch of a cast film in an ESR cavity and definition of (X_L, Y_L, Z_L), (X_C, Y_C, Z_C), and angle Φ. (b) Porphyrin orientation in the bilayer and the definition of angle $\bar{\theta}$, θ (angle for $g_{\parallel}$ and Z_C), and σ. (c) Normal (Gaussian) distribution function ($G(\theta)$) of the $g_{\parallel}$ axis around Z_C axis. See eq 3.

the ^{63}Cu and ^{65}Cu isotopes is taken into account. The nuclear quadrupole interaction and the nuclear Zeeman term are not considered. Angle $\bar{\theta}$ of the $\bar{g}_{\parallel}$ axis of the porphyrin complexes relative to the film axis Z_C is assumed to obey a Gaussian distribution function with a standard deviation of σ. The equations used for producing simulation spectra are given in the Experimental Section.

Figure 5 illustrates schematically the spatial arrangement of $\bar{g}_{\parallel}$ in a cast film. Φ and $\bar{\theta}$ denote the angle between the static magnetic field H_0 and the Z_C axis of a film and the angle between $\bar{g}_{\parallel}$ and the film Z_C axis, respectively. Φ is determined by the setting of a cast film in the ESR cavity, and $\bar{\theta}$ is estimated by comparison of observed and simulated spectra.

The major parameters in this simulation are $g_{\parallel}$, $g_{\perp}$, $A_{\parallel}$, $A_{\perp}$, $A^N_{\parallel}$, $A^N_{\perp}$, ν (frequency), $\bar{\theta}$, σ, and Φ. Among them, $g_{\parallel}$, $g_{\perp}$, $A_{\parallel}$, $A_{\perp}$, ν, and Φ are determined from the observed spectrum and the experimental conditions. The literature values were used for $A^N_{\parallel}$ and $A^N_{\perp}$. This is justified, as the ESR parameters of a particular Cu(II)–porphyrin derivative are identical in bilayers and in other matrices (see Table I). Thus, only $\bar{\theta}$ and σ remain as unknown parameters, and simulation spectra are produced for combinations of $\bar{\theta}$ and σ values.

Spectral Simulation and Orientation of Cu(PP) in a Cast Film of $2C_{14}$-Glu-ph-C_6-N^+. We carried out spectral simulation for wide variations of $\bar{\theta}$ and σ and obtained simulation spectra that are analogous to the observed spectra for the ranges of $35° < \bar{\theta} < 55°$ and $10° < \sigma < 20°$.

Figure 6 gives simulation spectra for the data of Figure 4a with different σ values. The film plane is set normal to the magnetic field ($H_0 \parallel Z_C$, $\Phi = 0.5°$[30]). The θ value is fixed at 45°. If σ is virtually zero ($\Phi = 0.5°$, Figure 6a), i.e., single-crystal-like, there

(28) Matsuda, Y., Department of Organic Synthesis, Faculty of Engineering, Kyushu University. Private communication.

(29) Chikira, M., Department of Industrial Chemistry, Faculty of Science and Technology, Chuo University. Private communication. Chikira, M.; Ando, K.; Kimura, M.; Nakabayashi, T.; Kondo, T.; Fujiwara, Y.; Kobayashi, N.; Shindo, H. *Abstr. 37th Conf. Coord. Chem. (Jpn.)* **1987**, 514.

(30) In the strict sense, the value of Φ (also $\bar{\theta}$ and σ) should be 0°, not 0.5°. We used the value of 0.5° to carry out calculations on the computer without error-stopping.

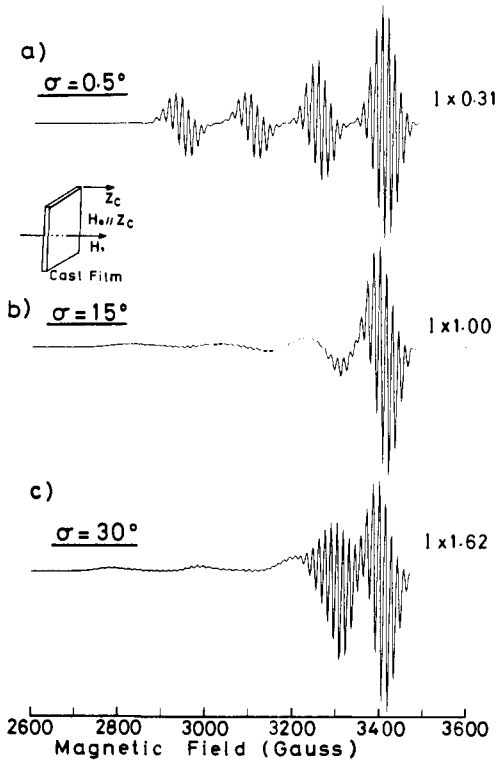

Figure 6. Influence of the value of the standard deviation σ on simulated spectra of Cu(PP) in a cast film at $\Phi = 0.5°$ and $\bar{\theta} = 45°$. The other parameters are the same as those in Figure 8. Key: (a) $\sigma = 0.5°$, (b) $\sigma = 15°$, (c) $\sigma = 30°$.

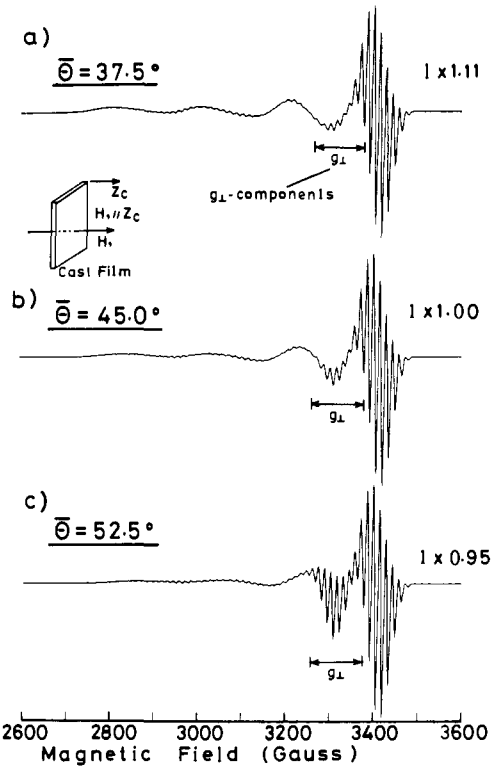

Figure 7. Influence of $\bar{\theta}$ value on simulated spectra of Cu(PP) in a cast film at $\Phi = 0.5°$ and $\sigma = 15°$. The other parameters are the same as those in Figure 8. Key: (a) $\bar{\theta} = 37.5°$, (b) $\bar{\theta} = 45.0°$, (c) $\bar{\theta} = 52.5°$.

exist 36 (=4 × 9) sharp signals due to the hyperfine coupling of the Cu nucleus ($I_{Cu} = {}^3/_2$) and the superhyperfine coupling of four nitrogen atoms. When $\sigma = 15°$, there are found large extra peaks at 3350–3450 G, broad, undulating $g_\parallel$ components at 2700–3200 G that do not show clear shfs, and weak $g_\perp$ components at 3250–3350 G. At an even larger standard deviation of $\sigma = 30°$, the intensity of the $g_\perp$ components is slightly enhanced. Among the three simulated spectra, Figure 6b ($\sigma = 15°$) agrees with the observed spectrum of Figure 4a reasonably well. Therefore, we subsequently examined the dependence by using this standard deviation.

Figure 7 shows the influence of the $\bar{\theta}$ variation (37.5–52.5°) on simulation spectra. The simulation was conducted for the case where the film plane was placed virtually normal ($\Phi = 0.5°$) to the magnetic field (see Figure 4a). Within the given variation, the spectra commonly display undulating $g_\parallel$ components at 2700–3250 G, $g_\perp$ components with clear N shfs, and large extra peaks at 3350–3470 G. The intensities of the $g_\perp$ components are sensitive to θ and increase with increasing $\bar{\theta}$ values. The observed spectrum of Figure 4a resembles a simulation spectrum of $\bar{\theta} = 45°$ particularly well.

Once we determine σ and $\bar{\theta}$, which are most appropriate for simulation of an observed spectrum, we can proceed to simulate the effect of disposition Φ of a cast film relative to the magnetic field. Three simulated spectra of Figure 8 correspond to the respective observed spectra of Figure 4. The dependence of the spectral pattern on Φ in the simulated spectrum is essentially identical with that in the observed spectrum.

From the preceding simulation data, we conclude that Cu(PP) molecules are placed in the cast film with the porphyrin plane oriented at 45° against the film plane. As mentioned above, the spacer and tail chains of $2C_{14}$-Glu-ph-C_6-N^+ are tilted against the bilayer plane by 45° and 65°, respectively. Cu(PP) is composed of a large hydrophobic plane (porphyrin ring) and two carboxylate groups. The diameter of the hydrophobic plane corresponds roughly to the spacer length of the amphiphile. Therefore, the porphyrin ring may be inserted into the hydrophobic spacer area along the molecular axis, and the carboxylate groups

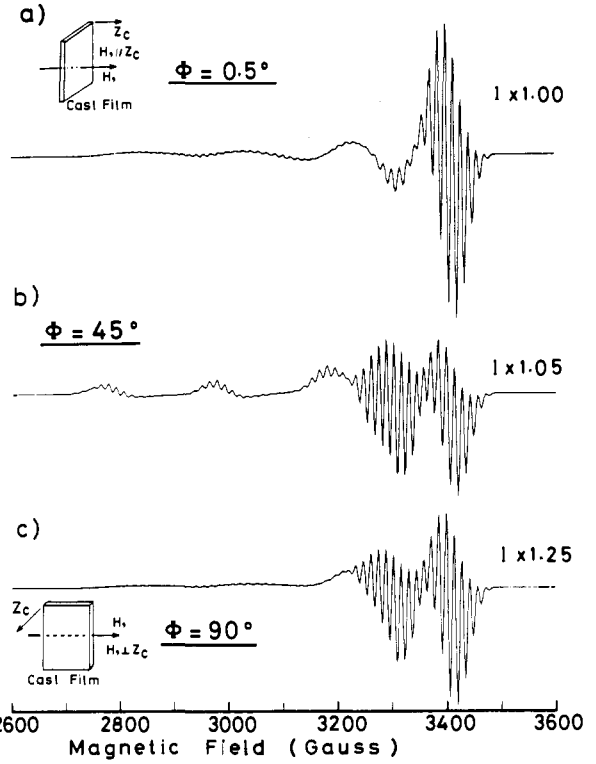

Figure 8. Most satisfactory simulation spectra obtained at $\bar{\theta} = 0.5°$, $\sigma = 15°$, $g_\parallel = 2.192$, $g_\perp = 2.050$, $A_\parallel = 201$ G, $A_\perp = 28$ G, $A^N_\parallel = A^N_\perp = 14$ G, $\Delta L_\parallel = 9$ G, $\Delta L_\perp = 8$ G (L's mean the peak to peak line-width parameter[34,39]), and $\nu = 9.455$ GHz. Key: (a) $\Phi = 0.5°$, (b) $\Phi = 45°$, (c) $\Phi = 90°$.

will readily form ion pairs with the ammonium head at the bilayer surface. This binding scheme is supported by the close agreement of the porphyrin orientation (45°) determined by the ESR simulation and the tilting of the spacer chain estimated by X-ray diffraction.

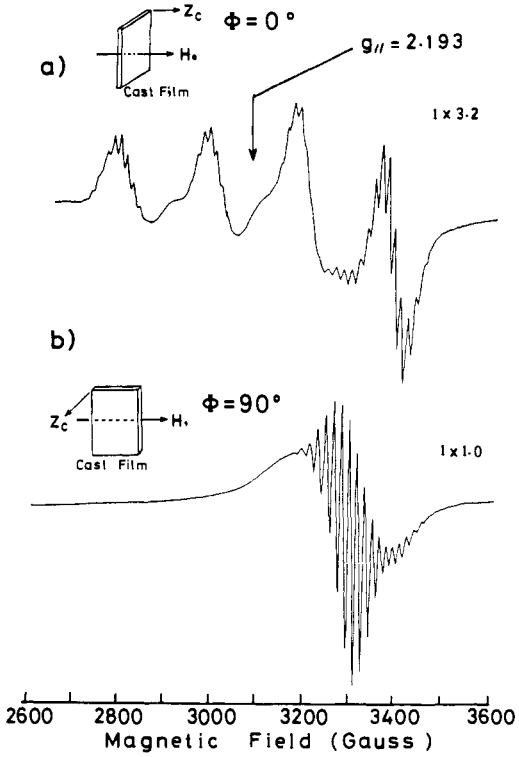

Figure 9. Observed ESR spectra of Cu(TPPS$_4$) embedded in a cast film of $2C_{14}$-Glu-ph-C_6-N^+: room temperature; ν = 9.4537 GHz; [Cu(TPPS$_4$)]:[$2C_{14}$-Glu-ph-C_6-N^+] = 1:80. Key: (a) $\Phi = 0°$, (b) $\Phi = 90°$.

Sources of Orientational Distribution and Disordering. The nonuniform orientation of porphyrins recognized in the experimental ESR spectra is attributed to orientational distribution and disordering. The orientational distribution is related to the statistical fluctuation of porphyrin orientation that can be defined by standard deviation (σ) in the normal distribution function. Its major sources are conceivably structural fluctuations of multilayers in a cast film and incomplete regularities of porphyrin binding. The X-ray diffraction pattern of a cast film is usually more diffuse than would be expected from the corresponding single crystal. Undulation of multilayers is always observed to some extent. In addition, the binding site in bilayers may not be fashioned in ideal complementarity with the structure of guest molecules and the porphyrin guest may be accommodated in nonuniform arrangements, even in a ideally regular multilayer. This produces an additional source of the spectral fluctuation.

There remains nonuniformities that cannot be explained by these sources in the form of standard deviations. The experimental and simulated spectra do not agree completely in the $g_\perp$-component region even after optimization of the σ and $\bar{\theta}$ values; compare Figures 4 and 8. This small discrepancy could arise from binding of Cu(PP) to disordered matrix regions. These structural defects cannot be excluded in the present procedure for preparation of cast films. Insufficient simulations can also contribute to this discrepancy.

Orientation of Cu(TPPS$_4$) in $2C_{14}$-Glu-ph-C_6-N^+ Bilayer, Comparison of Experimental and Simulated ESR Spectra. Subsequently, we examined the orientation of a second copper(II) porphyrin that has a different peripheral structure in terms of substituent and charge distribution. Figure 9 gives ESR spectra of a Cu(TPPS$_4$)-containing cast film in two different dispositions in the magnetic field. The observed ESR parameters are essentially identical with those obtained in the ligand matrix (Table I); thus, the original molecular structure of Cu(TPPS$_4$) is maintained in the cast film. The presence of the magnetic anisotropy between the two film dispositions is unmistakable. When the film plane is perpendicular to the magnetic field ($H_0 \parallel Z_C$, Figure 9a), four unsymmetrical signals of Cu hfs ($g_\parallel$ components) with nine additional signals of N shfs are predominant. The intensities of these peaks increase in the order $I_{Cu}(-^3/_2) < I_{Cu}(-^1/_2)$ $< I_{Cu}(+^1/_2)$, and $I_{Cu}(+^3/_2)$ shows a slight weakening. As the film is rotated around the X_L (X_c-) axis, the $g_\parallel$ components become weaker and the $g_\perp$ components and the extra peaks are intensified. When the film plane reaches a position parallel to the magnetic field (H_0) $\perp Z_C$, Figure 9b), the $g_\perp$ components with nine signals of N shfs and nine signals of extra peaks are solely observable. The in-plane rotation of the cast film does not affect the spectra at all.

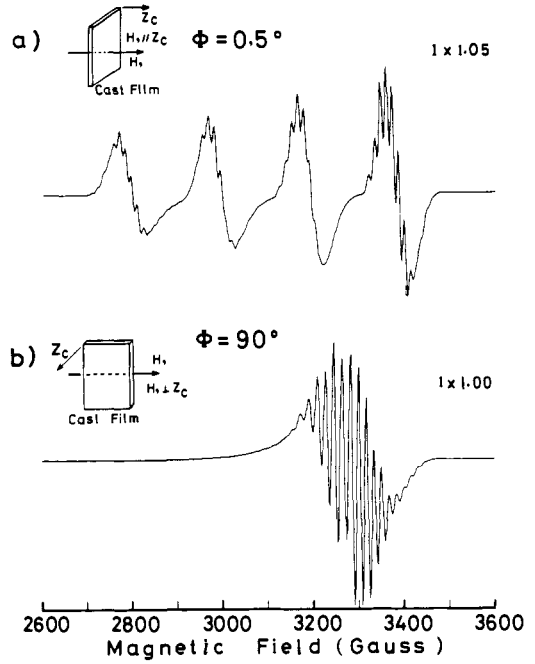

Figure 10. Most satisfactory simulation spectra obtained at $\bar{\theta} = 0.5°$, $\sigma = 15°$, $g_\parallel = 2.192$, $g_\perp = 2.050$, $A_\parallel = 197$ G, $A_\perp = 20$ G, $A^N{}_\parallel = A^N{}_\perp = 14$ G, $\Delta L_\parallel = 10$ G, $\Delta L_\perp = 8$ G, and $\nu = 9.4377$ GHz. Key: (a) $\Phi = 0.5°$, (b) $\Phi = 90°$.

During the course of the film rotation about the X_L axis, the $g_\parallel$ components and the $g_\perp$ components coexist and their relative intensities change with varying directions of the magnetic field (Φ). The observed spectral anisotropies are intrinsically the same as those observed for Cu(Tiron)$_2$ in our previous study.[21] The Cu(II)–porphyrin plane is disposed parallel to the plane of the cast film, and its $g_\parallel$ axis is parallel to the film Z_C axis. The orientation of the porphyrin plane within the film plane (X_C–Y_C plane) is random. When the cast film is placed parallel to the magnetic field ($H_0 \perp Z_C$), only the $g_\perp$ components appear. When the cast film is placed perpendicular to the magnetic field ($H_0 \parallel Z_C$), only the $g_\parallel$ components appear. The random orientation within the X_C–Y_C plane is not reflected in the ESR spectra because the $g_\parallel$ axis is parallel to the film Z_C axis.

Figure 10 gives simulation spectra of Cu(TPPS$_4$). It is assumed that σ is 15° and that the $g_\parallel$ axis of the porphyrin is virtually parallel ($\Phi = 0.5°$[30]) to the film Z_C axis. The two simulation spectra at $\Phi = 0.5$ and 90° are almost indistinguishable from the corresponding observed spectra of Figure 9. When Φ takes intermediate values between 0° and 90°, both of the $g_\parallel$ and $g_\perp$ components are observable in addition to the extra peaks and their relative intensities vary depending on the Φ value (the data not shown).

When the orientational fluctuation is assumed essentially nonexistent (i.e., $\sigma = 0.5°$[30]) as in single crystals, the signal shapes are completely different from those of the observed spectrum at $H_0 \perp Z_C$ as well as at $H_0 \parallel Z_C$: the individual signals of the single crystal sample are symmetrical and their intensities are identical. Therefore, better simulations are obtained with $\sigma = 15°$ rather than with $\sigma = 0.5°$. There remains still small differences between the observed and simulated spectra: the signal intensity ratio among four Cu hfs in the $H_0 \parallel Z_C$ spectrum and that at 3000–3200 G in the $H_0 \perp Z_C$ spectrum. These relatively small differences suggest again the presence of a small fraction of randomly oriented

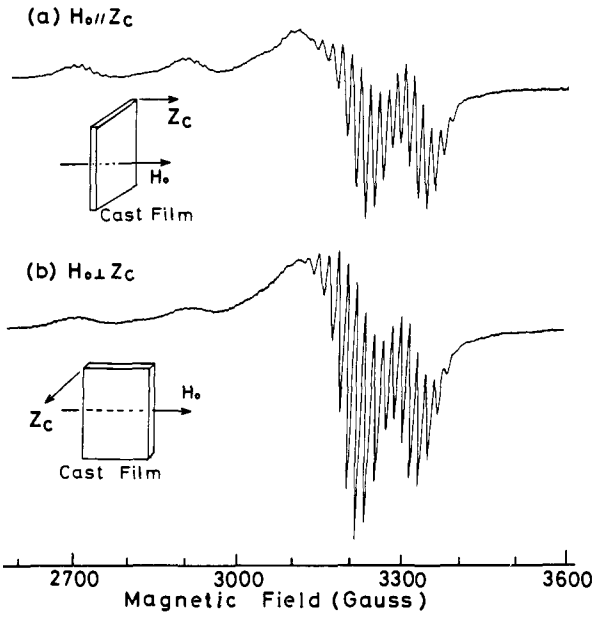

Figure 11. Observed ESR spectra of $Cu(TPPS_3)$ embedded in a cast film of $2C_{14}$-Glu-ph-C_6-N^+: room temperature; ν = 9.2210 GHz; [$Cu(TPPS_3)$]:[$2C_{14}$-Glu-ph-C_6-N^+] = 1:80. Key: (a) $\Phi = 0°$, (b) $\Phi = 90°$.

$Cu(TPPS_4)$ that does not obey the distribution function, as discussed previously for the Cu(PP) case.

The observed ESR anisotropy is consistent with the assumption that the symmetrical tetraanion of $Cu(TPPS_4)$ is placed flat on the surface of the cationic bilayer membrane. This disposition is in sharp contrast with the inserted arrangement of asymmetrically dianionic Cu(PP). This contrasting behavior necessitated extension of our ESR study to a trianionic porphyrin.

Macroscopic orientation of paramagnetic phthalocyanines has been accomplished by the Langmuir–Blodgett technique.[31-34] In particular, Palacin et al.[31] prepared LB films of an amphiphilic copper(II) porphyrazine and ω-tricosenoic acid, in which the porphyrazine ring stays horizontally on the substrate. Its anisotropic ESR spectra are indistinguishable from those of a cast film of $Cu(TPPS_4)/2C_{14}$-Glu-ph-C_6-N^+; compare Figure 9 in this paper with Figure 6 of ref 31. It is clear that cast films can provide anisotropic binding sites comparable to those of LB films.

Orientation of $Cu(TPPS_3)$ in the $2C_{14}$-Glu-ph-C_6-N^+ Bilayer. ESR spectra of trianionic $Cu(TPPS_3)$ in the same multilayer cast film are shown in Figure 11. Their ESR parameters (A and g values) are essentially identical with those of $Cu(TPPS_4)$; see Table I. The ESR anisotropy is rather small in Figure 11. The spectra contain the $g_\parallel$ and $g_\perp$ components and extra peaks, irrespective of the film disposition ($H_0 \parallel Z_C$ and $H_0 \perp Z_C$), although the $g_\perp$ components are enhanced by rotation from $H_0 \parallel Z_C$ to $H_0 \perp Z_C$. These data indicate that the orientation of $Cu(TPPS_3)$ molecules in the cast film is mostly random, though the parallel orientation (horizontal on the bilayer) is slightly more favored. This result is surprising if one considers the high regularity of the porphyrin orientation found in the preceding examples.

The random orientation will arise from the irregular layer structure of the cast film and/or from the irregular orientation of the porphyrin molecule in a regular multibilayer film. The molar ratio of porphyrins Cu(PP), $Cu(TPPS_4)$, and $Cu(TPPS_3)$ to the bilayer component is 1:60 to 1:80, and incorporation of such small amounts of porphyrins cannot disturb the overall regularity of the cast film. Furthermore, both Cu(PP) with two anionic substituents and $Cu(TPPS_4)$ with four anionic substituents give highly regular orientations. Therefore, trianionic $Cu(TPPS_3)$ should not destroy the overall regularity of the cast film. The *macroscopically* random orientation observed would be attributed to *microscopically* random disposition of $Cu(TPPS_3)$ onto the cationic bilayer membrane.

Factors That Determine the Molecular Orientation of Porphyrins in Cast Films of $2C_{14}$-Glu-ph-C_6-N^+. The ESR data described in the preceding sections can be justified by considering the supramolecular structure of the bilayer membrane and the molecular structure of porphyrins. The cast film possesses a highly regular multilayer structure. Within the individual layer, the ammonium amphiphiles are aligned with the molecular axis of 65 (the tail portion) and that of 45° (the spacer portion) against the membrane surface. Dianionic Cu(PP) molecules of type I are oriented against the membrane surface at an average angle of 45°. The tilt angle of the bilayer component and the porphyrin orientation give a remarkable agreement. The depth of the spacer portion along the methylene chain is estimated to be approximately 16 Å. The size of the planar Cu(PP) molecule is 12 Å × 14 Å × 16 Å, and the two carboxylate groups are located at the edge of the longest molecular axis. Therefore, the Cu(PP) molecule is apparently inserted into the bilayer in the spacer portion along the spacer methylene chain. The two carboxylates would be right at the bilayer surface and form stable ion pairs with surrounding ammonium head groups.

In contrast, tetraanionic $Cu(TPPS_4)$ (type III molecule) is placed horizontally on the bilayer membrane. This orientation produces the strongest electrostatic interaction between the porphyrin molecule and the cationic bilayer surface. Otherwise, the sulfonate unit has to be inserted into the hydrophobic bilayer interior.

The case of trianionic $Cu(TPPS_3)$ (type II molecule) is more complex. The ESR data show that this molecule is randomly oriented on the bilayer membrane. It cannot assume either of the above two orientations, since the full insertion as with Cu(PP) would place the sulfonate group in the hydrophobic interior and the horizontal placement as with $Cu(TPPS_4)$ would leave a hydrophobic corner of the porphyrin plane at the charged bilayer surface. A most probable arrangement for $Cu(TPPS_3)$ is shallow, much less regulated insertion into the membrane. Figure 12 illustrates schematically the binding modes of these porphyrins.

Orientation of Porphyrins in Bilayer Matrices of C_8-Azo-C_{10}-N^+. The molecular packing of bilayers plays a crucial role in controlling the orientation of bound porphyrins. It is therefore desirable to examine the influence of the bilayer structure on the porphyrin orientation. As mentioned previously, C_8-Azo-C_{10}-N^+ produces an interdigitated bilayer structure and the molecular axis is essentially normal to the bilayer surface.

In the first place, Cu(PP) was dispersed in a cast film of C_8-Azo-C_{10}-N^+ in a molar ratio of 1:58. This ratio is the same as that used for the data of Figure 4. ESR spectra of the cast film are broad, and it is not possible to infer the porphyrin orientation from these data (the data not shown). This broadening is conceivably caused by aggregation of Cu(PP) molecules.

Trianionic Cu(ChP) that should be more dispersible in the cationic bilayer was subsequently examined. In Figure 13, Cu hfs and N shfs are clearly noted, and it is indicated that Cu(ChP) is molecularly dispersed in this cast film. When the film plane is parallel to the magnetic field ($H_0 \perp Z_c$), the $g_\parallel$ components are slightly stronger than the $g_\perp$ components, and when the film plane is perpendicular, the reverse is true. Therefore, the vertical insertion of Cu(ChP) into the bilayer appears to be slightly more favored than the horizontal attachment. However, the average orientation is close to being random.

ESR spectral data of $Cu(TPPS_3)$ and $Cu(TPPS_4)$ are summarized in Figure 14. These two porphyrins display very similar modes of magnetic anisotropy. When the film plane is perpendicular to the magnetic field ($H_0 \parallel Z_C$), the $g_\parallel$ components are predominant. The $g_\perp$ components become predominant if $H_0 \perp Z_C$. These ESR patterns are closely related to those observed for $Cu(TPPS_4)$ in Figure 9 and indicate that both $Cu(TPPS_3)$ and $Cu(TPPS_4)$ are placed horizontally on the bilayer surface. The porphyrin orientations in the bilayer of C_8-Azo-C_{10}-N^+ are illustrated in Figure 15.

(31) Palacin, S.; R-Teixier, A.; Barraud, A. *J. Phys. Chem.* **1986**, *90*, 6237.
(32) Palacin, S.; R-Teixier, A.; Barraud, A. *J. Phys. Chem.* **1989**, *93*, 7159 and refs 2–9 cited therein.
(33) Pace, M. D.; Barger, W. R.; Snow, A. W. *Langmuir* **1989**, *5*, 973.
(34) Pace, M. D.; Barger, W. R. *J. Magn. Reson.* **1987**, *75*, 73.

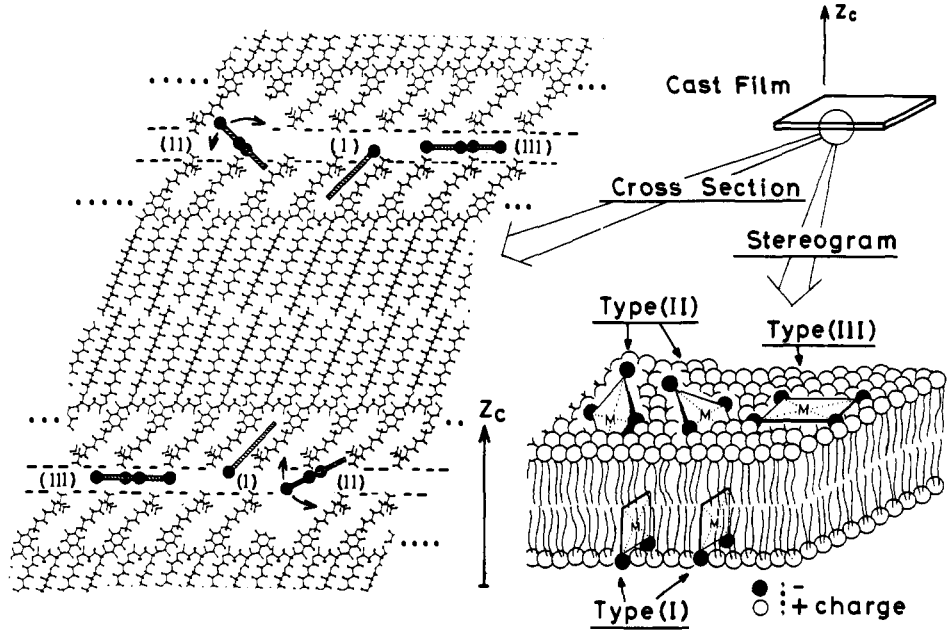

Figure 12. Schematic representation of three types of anionic porphyrins in a cast multibilayer film of $2C_{14}$-Glu-ph-C_6-N^+. The overall bilayer organization is assumed to be the same as that of Figure 3. For clarity, counterions are not shown and the bilayer units are separated from each other. The spacer portion is also not shown in "Stereogram". Type I porphyrins are inserted into the bilayer along the molecular axis of the spacer chain. Type II porphyrins are randomly placed on the bilayer surface. Type III porphyrins lie flat on the bilayer.

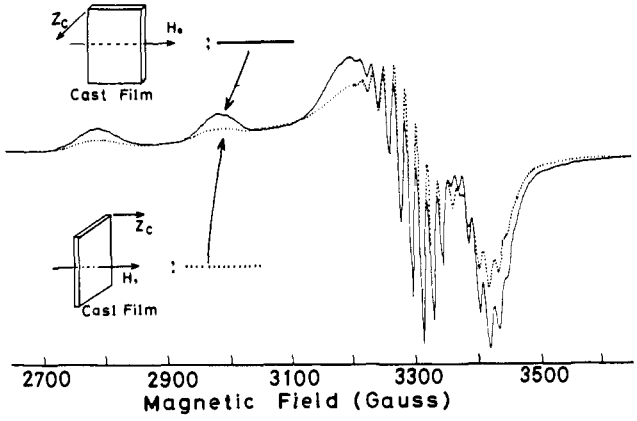

Figure 13. Observed ESR spectra of Cu(ChP) embedded in a cast multibilayer film of C_8-Azo-C_{10}-N^+: room temperature; ν = 9.4554 GHz; [Cu(ChP)]:[C_8-Azo-C_{10}-N^+] = 1:80. Key: —, Φ = 90°; ---, Φ = 0°.

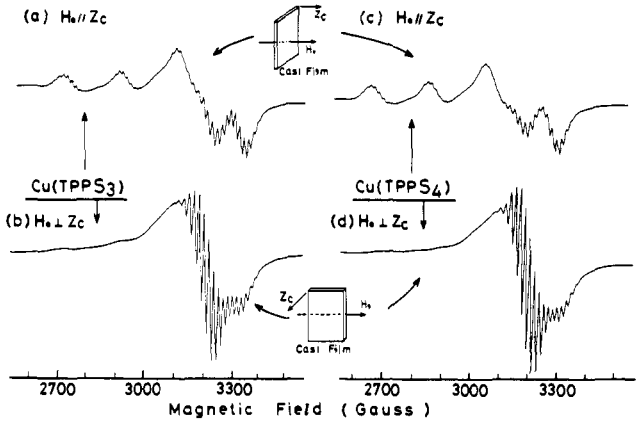

Figure 14. Observed ESR spectra of $Cu(TPPS_3)$ and $Cu(TPPS_4)$ in a cast film of C_8-Azo-C_{10}-N^+: room temperature; [porphyrin]:[C_8-Azo-C_{10}-N^+] = 1:80; ν = 9.222 GHz. Key: (a) and (b) $Cu(TPPS_3)$, (c) and (d) $Cu(TPPS_4)$.

The porphyrin orientations observed in a cast film of the single-chain amphiphile present an interesting difference from the orientations observed in a cast film of the double-chain amphiphile. The interdigitated molecular packing seems to be too tight for incorporation of porphyrin guests into the hydrophobic interior. When sufficient numbers of the negative charge are attached to the periphery of the porphyrin ring, porphyrin molecules are placed horizontally, even if some hydrophobic corners are exposed to the polar environment.

Conclusion

In the present study, we made quantitative estimates of the spatial arrangement of anionic porphyrins in matrices of ammonium bilayer membranes. An elaborate computer simulation of ESR spectra was necessary for this purpose. The spatial arrangements are determined by the molecular structure of guest porphyrins and the supramolecular structure of host bilayers. The mode of the spatial arrangements and its quantitative parameters, $\bar{\theta}$ and σ, are summarized in Table II. The molecular organizations of the host bilayer are not reflected in the porphyrin orientation ($\bar{\theta}$) in the case of the type III guest. This is readily understood, since the symmetrically tetrasubstituted porphyrins are placed horizontally on the bilayer surface. The molecular alignment within the bilayer is not relevant to the orientation of this guest.

Table II. Orientation of Porphyrin Guests in Host–Bilayer Membranes[a]

bilayer membrane	C_8-Azo-C_{10}-N^+ (interdigitated bilayer)	$2C_{14}$-Glu-ph-C_6-N^+ (tilted bilayer)
type I Cu(PP)	random	tilted (45°, 15°)
type II $Cu(TPPS_3)$	horiz (0°, 15°)	random
type III $Cu(TPPS_4)$	horiz (0°, 15°)	horiz (0°, 15°)

[a] Relative orientation to layer plane. The $\bar{\theta}$ and σ values are given in parentheses.

On the other hand, the orientations of type I and type II porphyrins are dependent on the mode of bilayer assemblage. The $2C_{14}$-Glu-ph-C_6-N^+ bilayer accommodates type I porphyrins in the spacer area along the methylene alignment, whereas this accommodation is not possible for the interdigitated bilayer of C_8-Azo-C_{10}-N^+. Type II porphyrins are not able to penetrate at all into the interdigitated bilayer, hence the horizontal incorporation. The bilayer of $2C_{14}$-Glu-ph-C_6-N^+ appears to allow partial incorporation of this guest, giving random porphyrin orientation.

The value of σ, a measure of orientational distribution was invariably 15°, except for the case of random orientation where σ cannot be determined. This implies that the distribution is not

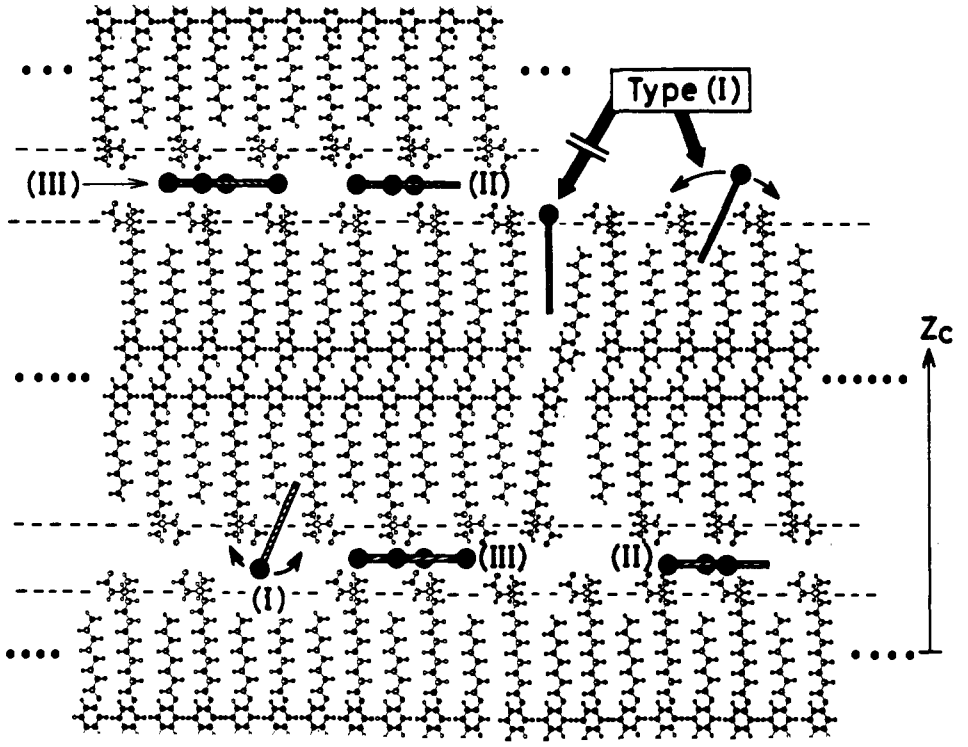

Figure 15. Schematic representations of three types of anionic porphyrins in a cast multibilayer film of C_8-Azo-C_{10}-N^+. For simplicity, counterions are not shown. The bilayer packing is based on the X-ray diffraction data. Type I porphyrins assume random orientations. Type II and III porphyrins stay horizontally on the bilayer surfaces.

produced by insufficient structural complementarity of host and guest. Cast multibilayer films usually show undulating structures, as observed by scanning electron microscopy. We believe this flexibility of the layer structure is responsible for the orientational distribution. Thus, it is concluded that porphyrin binding is precise at the molecular level.

Similar orientational control is observed for porphyrins given in Chart III. The geometrical distribution (but not the number) of the negatively charged substituent determines the porphyrin orientation.

The present study established the basic methodology of the control of porphyrin orientation in the bilayer assembly. This methodology should be quite useful for designing biomimetic functional systems that contain multiple porphyrin units in spatially defined orientations.

Experimental Section

Materials. C_8-Azo-C_{10}-N^+ was prepared according to the procedure of Shimomura et al.[35]

Ditetradecyl Glutamate Hydrochloride. Tetradecan-1-ol (63.4 g, 0.296 mol), L-glutamic acid (19.6 g, 0.133 mol), and *p*-toluenesulfonic acid monohydrate (38.0 g, 0.20 mol) were suspended in 300 mL of toluene at room temperature, and the solution was refluxed for 7 h with a Dean-Stark trap. The homogeneous reaction mixture was then washed with aqueous K_2CO_3 (~0.2 M, 200 mL × 2) and water (300 mL × 3). The solvent was removed in vacuo, and the colorless residue was dissolved in 150 mL of acetone. Colorless precipitates that were formed by addition of 35% hydrochloric acid (12 mL) on ice were recrystallized from acetone: colorless powder; mp 83.0 → 91.0 °C (arrow indicates the liquid crystalline temperature range); yield 46.0 g (60%); IR (Nujol) ν(C=O) 1750 cm^{-1}.

4-[(6-Bromohexyl)oxy]benzoic Acid. In 600 mL of ethanol that contains 26.0 g (0.40 mol) of KOH were added ethyl 4-hydroxybenzoate (55.0 g, 0.33 mol) and 1,6-dibromohexane (211 g, 0.86 mol). The mixture was refluxed for 7 h and filtered while it was hot. The solvent and excess 1,6-dibromohexane were removed in vacuo. The oily brown residue [TLC (silica gel, $CHCl_3$) R_f = 0.7; IR (CCl_4) ν (C=O) 3320, ν (Ph) 1610, 1505 cm^{-1}] was dissolved in a mixture of 500 mL of acetic acid, 200 mL of 30% hydrobromic acid, and 100 mL of ethanol, and the solution was refluxed for 7 h. The precipitates formed on ice cooling and were collected, washed with water, and recrystallized from benzene/hexane:white powder; yield 47% (32.5 g): mp 136 → 149 °C; TLC (silica gel, $CHCl_3$) R_f = 0.59, single spot; IR (CCl_4) ν(C=O) 1685 cm^{-1}.

Ditetradecyl *N*-[4-[(6-Bromohexyl)oxy]benzoyl]-L-glutamate. The O,O′-substituted glutamic acid hydrochloride (5.0 g, 8.7 mmol), triethylamine (1.8 g, 17 mmol), and diethyl phosphocyanide (90%, 3.2 g, 17 mmol) were dissolved in 100 mL of dry tetrahydrofuran (THF) on an ice bath, and [(6-bromohexyl)oxy]benzoic acid (3.0 g, 10 mmol) in 30 mL of THF was added dropwise in 20 min with stirring by keeping the temperature below 5 °C. After the solution was stirred for 1 day at room temperature, precipitates of triethylamine hydrochloride and the solvent were removed. Recrystallization of the residue from methanol gave a colorless powder in 86% yield (6.2 g): mp 63–64 °C; TLC (silica gel, $CHCl_3$) R_f = 0.71; IR (CCl_4) ν(N-H) 3320, ν(C=O) 1730, 1640, ν(Ph) 1610, 1505 cm^{-1}.

Chart III

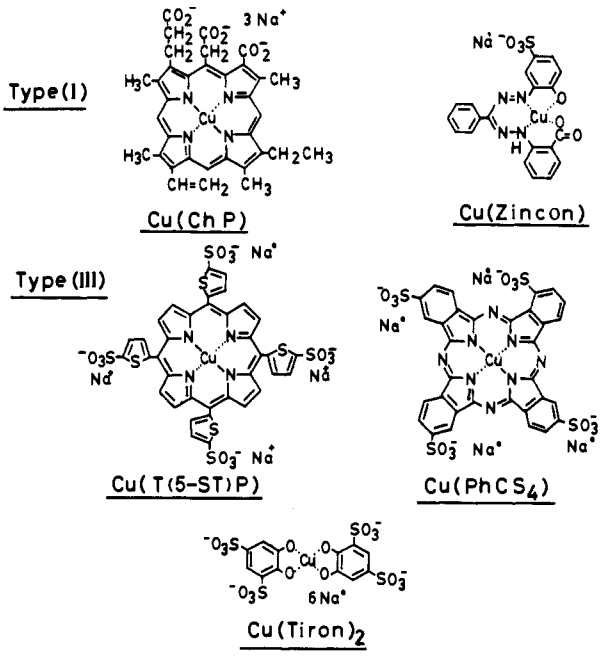

(35) Shimomura, M.; Ando, R.; Kunitake, T. *Ber. Bunsen-Ges. Phys. Chem.* **1983**, *87*, 1134.

Ditetradecyl N-[4-[[6-(trimethylammonio)hexyl]oxy]benzoyl]-L-glutamate Bromide. The preceding product (2.5 g, 3 mmol) was dissolved in 50 mL of dry benzene, and trimethylamine gas (bp 2.9 °C, 1 g, 17 mmol) was introduced by bubbling. The reaction vessel was sealed with Teflon film. After the solution was stirred for 5 days at room temperature, the solvent and excess trimethylamine were removed in vacuo. Recrystallization of the colorless residue from acetone/ethyl acetate gave white powder in 82% yield (2.2 g): mp 60 → 210 °C; ^{1}H NMR ($CDCl_3$/TMS) CCH_3 0.88 (t, 6 H), CCH_2C 1.26 (m, θ 0 H), N^+CH_2 1.92 (m, 2 H), $COCH_2C$ 2.35 (m, 2 H), N^+CH_3 3.39 (s, 9 H), OCH_2 3.7 ~ 4.3 (m, 6 H), NCH 4.74 (d, 1 H), ArH, NH 6.7 ~ 7.9 (d, d, 5 H) ppm. Anal. Calcd for $C_{49}H_{91}N_2O_3Br$: C, 65.38; H, 10.19; N, 3.11. Found: C, 64.94; H, 10.14; N, 3.05.

Preparation of Cu(II)–Porphyrin Derivatives. Cu(ChP), Cu($PhCS_4$), and PP from Aldrich Chemical Co. were used without further purification. $TPPS_4$, T(5-ST), and $TPPS_3$ were obtained from Dojin Chemicals. Commercial porphyrins (1.1×10^{-6} mol) in 100 mL of deionized water were mixed with aqueous $CuSO_4$ (0.1 M, 10 μL). The solutions were adjusted to pH 6.5–7.5 with 0.1 N NaOH, warmed to ~70 °C for 10 min, and used immediately for doping of multibilayer cast films.

Preparation of Cast Multibilayer Films Doped with Copper(II) Porphyrins. To hot aqueous solutions of copper(II) porphyrins (1.1×10^{-6} mol/100 mL) was added 0.08–0.10 g ($(9.0–11) \times 10^{-5}$ mol) of powdery amphiphiles, and the mixtures were sonicated at 70–80 °C (above Tc[36]) for 5 min with a Bransonic Cell Disruptor 185 (sonic power 40). Water was evaporated, and the residues were sonicated again in 2 mL of deionized water at ~70 °C for 3 min to obtain turbid dispersions. However, a mixture of Cu(PP) (1×10^{-5} M) and the bilayers (1×10^{-3} M) could not be made completely homogeneous. Remaining brown particles were removed from the hot mixture by filtration with a cellulose acetate filter (pore size, 0.45 μm).

Hot aqueous bilayer dispersions (~50 mM, 2 mL) that contain copper porphyrins were spread on flat Teflon sheets (Fluoropore FP-010, Sumitomo Electric) that were surrounded by square templates made of a hydrophilic photographic negative film of 2.5 cm × 3.0 cm size. The templates were used in order to shape square cast films. The dispersions gelatinized at room temperature (25–30 °C) were allowed to stand as such. A few days later, cast films of ~0.05-mm thickness resulted. This thickness corresponds to ca. 10000 bilayers. These cast films held in a guide template could be easily peeled from the Teflon sheet.

ESR and X-ray Measurement. ESR spectra of the cast films were obtained at ~20 °C with a JEOL JES-FEIXG X-band spectrometer with 100-kHz magnetic field modulation, 5-mW microwave power, and 6.3-G modulation amplitude. The magnetic field and the microwave frequency were measured by an Echo Electronics EFM-2000 NMR field counter and an Advantest TR5213 microwave counter, respectively. A quartz rod (5 mm × 30 cm) that is shaped into a flat plate (5 mm × 30 mm) at an end was used as a sample holder. A cast film (2.5 cm × 3 cm) was cut into ca. five pieces (4 mm × 25 mm), and they were stacked and fixed by pressing gently or by applying grease. The stacked film was mounted, by use of grease, on the flat portion of the ESR rod. The rod was mounted vertically in the cavity of the ESR spectrometer and rotated to observe the magnetic anisotropy of the sample.

The X-ray diffraction (θ–2θ scattering reflection method) was carried out on a Rigaku Denki Rotaflex RAD-R-32 at room temperature. The width of divergence and the scattering slit were fixed by $^1/_6°$, and the area of the sample film was 1.5 cm × 2.0 cm.

Fundamental Equations for ESR Simulation Program. Relationships of the Coordinate Systems. For the calculation of ESR spectra, one has to make clear relationships among the coordinate-axis systems. Here, we use three-coordinate systems; laboratory axes (X_L, Y_L, Z_L), cast-film axes (X_C, Y_C, Z_C), and the principal g axes (X_g, Y_g, Z_g). Figure 16 shows the relationships among these three systems. These systems coincide with each other by system rotation. In the cast-film axes, the Z_C direction is perpendicular to the cast-film plane. The X_C and Y_C axes are along the edges of the cast film, and the X_c axis is coincident with the X_L axis (Figure 16a,b). The static magnetic field H_0 and the rotation axis of the cast film are set up by a human hand along the Z_L axis and $X_L(=X_c)$ axis, respectively (Figure 16a,b). The rotation angle of the cast film about the X_L is defined by Φ. Namely, Φ is the angle between the Z_C axis and H_0.

The principal g axes (X_g, Y_g, Z_g) of copper porphyrins are defined by the Euler angles α and θ in the cast-film system (X_C, Y_C, Z_C). α represents rotation of the (X_C, Y_C, Z_C) system about the Z_c axis, and θ is the rotation angle of the (X'_C, Y'_C, Z'_C) system about the Y'_C axis. The $\bar{Z}_g$ axis represents the mean direction ($\bar{g}_\parallel$) of the $g_\parallel$ axes with the standard deviation σ. Namely, the angle $\bar{\theta}$ is the mean tilt angle of the $\bar{g}_\parallel$ axis from the cast-film Z_C direction.

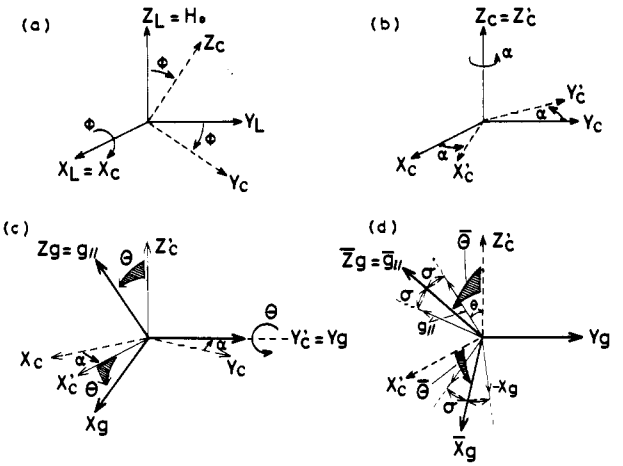

Figure 16. Transformation of coordinate systems and definition of angle Φ, α, θ, σ, and $\bar{\theta}$ for computer calculation: (a) rotation of Φ, from laboratory axes to cast film axes; (b) and (c) rotation of the Eularian angles α and θ, from cast-film axes to g axes (X_g, Y_g, Z_g); (d) distribution of θ around $\bar{g}_\parallel$ ($=Z_g$) axis with a standard deviation σ.

Resonance Magnetic Field. The resonance magnetic field H_R (G) was calculated by the standard equation,[33,37,38] which includes the zero-order Zeeman term, the first- and second-order hyperfine interaction, and the first-order superhyperfine interaction with four ^{14}N nuclei of the ligand. The nuclear quadrupole interactions and nuclear Zeeman term are neglected. For simplicity, we assumed that the principal $A(^{63}Cu,^{65}Cu)$ axes and the principal $A^N(^{14}N)$ axes coincide with the principal g axes. The A and A values of ^{65}Cu isotope could not be estimated precisely from the experimental spectra due to signal overlapping with the major signal of the ^{63}Cu isotope. Hence, the A and A values of ^{65}Cu were estimated from

$$A(^{65}Cu) = A(^{63}Cu)(^{65}\gamma/^{63}\gamma) \quad (1)$$

where γ denotes the nuclear magnetogyric ratio of Cu with $^{65}\gamma/^{63}\gamma$ = 1.0743.

The direction cosines l_x, l_y, and l_z of the static magnetic field H_0 in the principal g axes can be expressed as eq 2.[39]

$$\begin{aligned} l_x &= -\cos\theta \sin\alpha \sin\Phi - \sin\theta \cos\Phi \\ l_y &= -\cos\alpha \sin\Phi \\ l_z &= -\sin\theta \sin\alpha \sin\Phi + \cos\theta \cos\Phi \end{aligned} \quad (2)$$

Spectrum Line Shape. We use eq 3[29,34] as the line-shape function, $S(H)$, of the first-derivative ESR spectra. In eq 3, $G'(H-H_R)$ represents the first derivative of the Gaussian line-shape function and $G(\theta)$ is the normal (Gaussian) distribution function having a mean tilt angle θ with standard deviation σ. The g_p denotes the angular dependence of the transition probability.

$$S(H) = \int_\alpha \int_\theta G'[H-H_R(\Phi,\alpha,\theta)] g_p \sin\theta\, G(\theta)\, d\theta\, d\alpha \quad (3)$$

The resonance positions were calculated from 2600 to 3600 G for every 2 G, and the intensities were obtained by using eq 3 for α and θ from 1° to 180° at every 1°.

Acknowledgment. We are grateful to Dr. Yoshihisa Matsuda of this department for his advice and discussion on the simulation program (spectral line shape) and the experimental technique of the anisotropic ESR measurement. Dr. Makoto Chikira of Chuo University generously provided us with a computer program for calculation of the resonance position. We also thank Dr. Hideo Okada and Dr. Satoshi Ozawa for advice on the programming, Mr. Hideki Horiuchi for skillful preparation of ESR quartz cells, and Mr. Shinji Tsukamoto for his synthesis of $2C_{14}$-Glu-ph-C_6-N^+.

(36) The gel to liquid crystal phase transition of the C_8-Azo-C_{10}-N^+ bilayer (sonicated sample, 10 mM) occurs at 68 °C (T_c) with ΔH = 47 kJ/mol, and T_c of the $2C_{14}$-Glu-ph-C_6-N^+ bilayer is 51 °C with ΔH = 54 kJ/mol.

(37) Taylor, P. C.; Baugher, J. F.; Kriz, H. K. *Chem. Rev.* **1975**, 203. Mattar, S. M. *J. Phys. Chem.* **1989**, *93*, 791.
(38) Rollmann, L. D.; Chan, S. I. *J. Chem. Phys.* **1969**, *50*, 3416.
(39) The parameters l_x, l_y, and l_z were introduced according to the procedure of Van et al.: Van, S. P.; Birrell, G. B.; Griffith, O. H. *J. Magn. Reson.* **1974**, *15*, 444.
(40) Lin, W. C. In *The Porphyrins, Vol. IV, Physical Chemistry, Part B*; Dolphin, D., Ed.; Academic Press: New York, 1979; p 360.